A TRANSTHALAMIC PATHWAY IS CRUCIAL FOR STIMULUS FEATURE SELECTIVITY IN HIGHER ORDER CORTEX

Authors: C. Mo[1,2], C. McKinnon[1], Masaki Makitani[1], S. M. Sherman[1]
Affiliations: [1]Department of Neurobiology, University of Chicago, Illinois, USA
[2]The Florey Institute of Neuroscience and Mental Health, University of Melbourne, Victoria, Australia

ABSTRACT

Sensory perception arises from activity between cortical areas, first primary cortex and then higher order cortices. This communication is served at least in part by transthalamic (cortico-thalamo-cortical) pathways, which ubiquitously parallel direct corticocortical pathways, yet their role in sensory processing has largely been ignored. Here, we show that the transthalamic pathway from S1 to S2 propagates task-relevant information required for correct sensory decisions. Using optogenetics, we specifically inhibited the pathway at its synapse in higher order somatosensory thalamus of mice performing a texture-based discrimination task. At the same time, the cellular effects of inhibition were monitored in primary or secondary cortex using two-photon calcium imaging. Inhibition severely impaired performance in a delayed discrimination task, despite intact direct corticocortical projections, thus challenging the purely corticocentric map of perception. Interestingly, the inhibition did not reduce overall cell responsiveness to texture stimulation in somatosensory cortex, but rather disrupted the texture selectivity of cells, a discriminability that develops over task learning. This discriminability was more disrupted in the secondary than primary somatosensory cortex, emphasizing the feedforward influence of the transthalamic route. Transthalamic pathways thus appear critical in delivering performance-relevant information to higher order cortex and are critical hierarchical pathways in perceptual decision-making.

INTRODUCTION

The brain processes sensory signals in hierarchical order with primary sensory cortex activated before secondary cortex (Felleman and Van Essen, 1991). The information from primary to secondary cortex can arrive either directly or indirectly via higher order thalamic nuclei. These feedforward cortico-thalamo-cortical, or transthalamic, pathways often if not always are present in parallel to direct pathways and use 'driver' type synapses that support the fast, robust propagation of stimulus information through sensory pathways (Sherman and Guillery, 1998, 2013; Sherman, 2016; Usrey and Sherman, 2021; Miller-Hansen and Sherman, 2022). Feedforward transthalamic pathways are thus well positioned to influence higher order processing. Yet they are absent in many models of perceptual processing (Felleman and Van Essen, 1991; Roland et al., 2014; Hilgetag and Goulas, 2020; Vezoli et al., 2021) and also absent in standard textbook views of thalamocortical relationships (e.g., Fig. 4.51B of (Luo, 2020), Fig. 28-2 of (Kandel et al., 2000), and Figs. 25.12 and 27.15 of (Squire et al., 2008).

There is some evidence to suggest that these indirect pathways are surprisingly powerful inputs to higher order cortex (Theyel et al., 2010) and carry distinct, task-relevant information, compared to the direct cortical projections (Takahashi et al., 2020; Blot et al., 2021; Musall et al., 2023). In the mouse somatosensory brain slice, the transthalamic pathway can strongly activate secondary cortex in the absence of the corticocortical pathway (Theyel et al., 2010). In mice moving through a visual environment, it is the thalamocortical input rather than the corticocortical input that has a stronger influence on the response patterns of higher order cortex (Blot et al., 2021). During a whisker-based perceptual task, activating the transthalamic-projecting apical dendrites of primary somatosensory cortical cells enhanced whisker-based detection, but activating the corticocortical-projecting dendrites had no behavioral impact (Takahashi et al., 2020). It thus appears that the transthalamic pathway is a key contributor to cortical processing, but it is not clear what information propagates through this pathway to higher order cortex. Here we show that the feedforward transthalamic pathway is essential for discrimination of stimulus features in cortex and correct perceptual decisions.

We tested the function of the transthalamic pathway in the whisker system of the mouse by using optogenetic inhibition of layer 5 (L5) terminals in higher order thalamus from primary somatosensory cortex (S1). We observed the effects of this inhibition on the animals' ability to perform a whisker-based discrimination task that relies on cortical communication (Helmchen et al., 2018; Park et al., 2022). We concurrently assessed neuronal responses in S1 and secondary somatosensory cortex (S2) using 2-photon calcium imaging. Importantly, instead of suppressing the pathway during the entire trial (Chen et al., 2016; Takahashi et al., 2020; Qi et al., 2022), which limits interpretation regarding perceptual processing, we separately inhibited during the period of sensory whisking and a delay epoch separating sensation and motor response. We found that texture discrimination performance was impaired by inhibition during both the sensory and delay periods, and inhibition during the sensory epoch also disrupted cell selectivity for the rewarded texture in S2, with smaller effects on cells in S1. Transthalamic pathways thus appear critical in delivering performance-relevant information to higher order cortex, and are powerful but underappreciated hierarchical pathways in perception.

RESULTS

BEHAVIORAL EFFECTS OF SUPPRESSING THE TRANSTHALAMIC PATHWAY

Performance on a Discrimination Task

To test the behavioral effect of inhibiting the somatosensory transthalamic pathway, we used a texture discrimination task, which requires S1 to S2 corticocortical communication (Chen et al., 2016; Helmchen et al., 2018; Park et al., 2022) (**Fig. 1A**). Textures were presented to the whisker fields of water-restricted, head-fixed mice, who indicated their discrimination choice by a lick or no-lick response in a go/no-go task design (**Fig. 1B**). A lick response to a texture with a coarse grating (Grating 5, G5) was rewarded with a drop of water (Hit). A lick response to a smooth texture made of foil (Grating 0, G0) was punished with an alarm and 12 sec timeout (False alarm). No-lick responses to G5 were regarded as a Miss, whilst no-lick to G0 was a Correct Rejection (CR). A delay of 1 sec separated the texture presentation 'sensory period' of the task from the 'response period' and subsequent 633nm laser inhibition via the Jaws opsin could be applied during the sensory or delay epochs (**Fig. 1C**). Mice generally required 3-4 weeks to successfully discriminate G5 from G0, defined as a d-prime performance above 1 for 2 consecutive days (**Fig. 1D**). After G5 vs G0 discrimination, psychometric performance was tested by presentation of textures with gratings of lower coarseness (G4-G1) (**Fig. 1E**).

Inhibiting S1 Layer 5 to POm terminals. Cortical L5 cells that project to higher order thalamus are the sources of transthalamic pathways. We targeted the projection from S1 L5 by injecting a Cre-dependent adeno-associated virus (AAV) carrying the inhibitory opsin, Jaws, into S1 of layer 5 Cre (Rbp4) mice. An optic fiber was implanted in the higher order thalamic nucleus, the posterior medial nucleus (POm) to target inhibition of S1 L5 to POm terminals (**Fig. 1F**). The implant was in the anterior-dorsal part of POm, which receives terminals from S1 L5 and contains cells that project to the upper layers of S2 (**Suppl Fig. 1**). We verified that activity of S1 L5 to POm terminals could be suppressed by Jaws activation there for at least 2 sec (**Fig. 1G**, **Suppl Fig. 2**).

To locate S1 and S2, we mapped hemodynamic changes to stimulation of the whiskers using intrinsic signal optical imaging of cortex through a cranial glass window (**Fig. 1H**). By overlaying the images of whisker response maps and expression of Jaws-TdTomato in S1 L5, we could exclude any mice with expression which had spread to S2. The overlay also allowed identification of any S1 barrels which did not localize with the expression of Jaws, the corresponding whiskers of which were trimmed if they contacted the texture during the task (**Fig. 1H**). Thus, any whiskers that could contact the texture and contribute to task performance had their neural representation in S1 modifiable by the Jaws opsin.

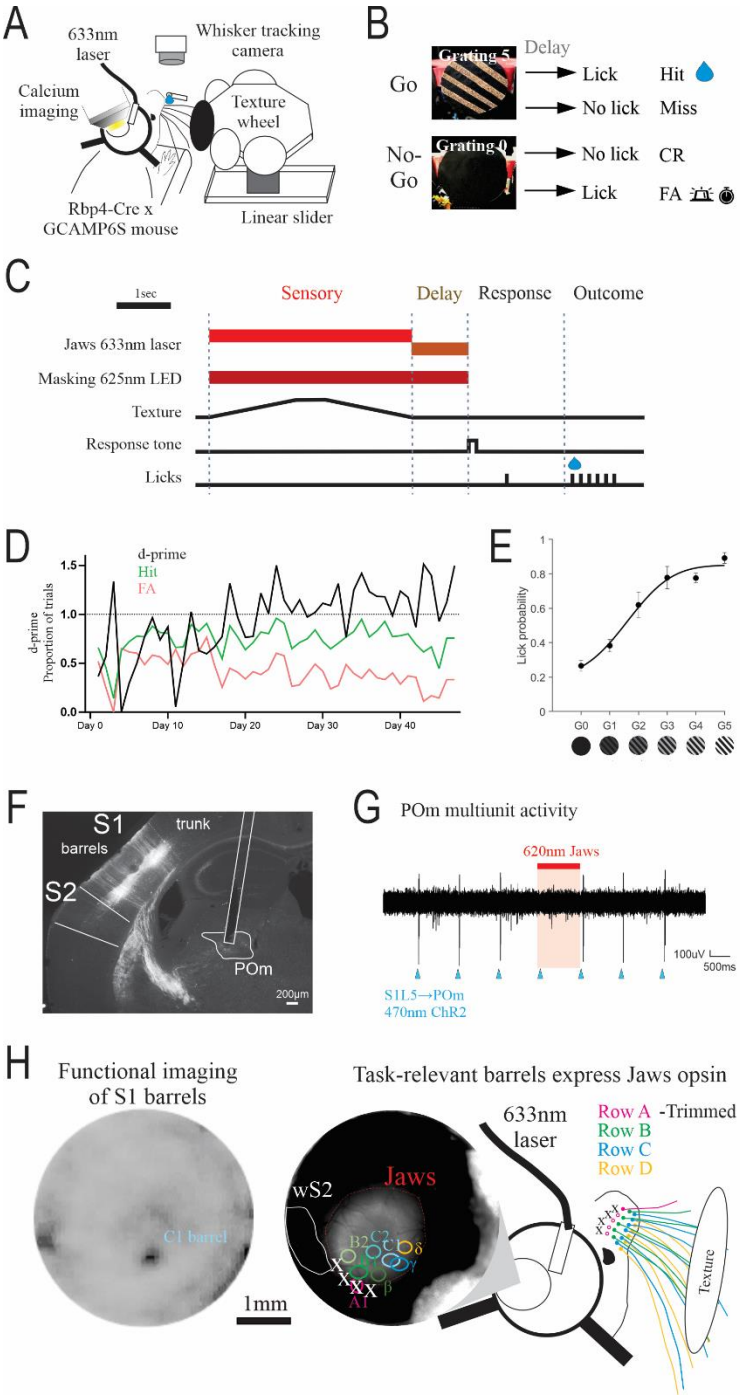

Figure 1. Targeting the S1 L5 transthalamic pathway in a discrimination task.

(**A**) Schematic of discrimination task, optogenetic inhibition, calcium imaging and whisker tracking.

(**B**) Go/no-go discrimination task design. Rewarded texture is one with gratings (G5), punished texture is smooth foil (G0).

(**C**) Time course of a trial with a Hit outcome. For laser inhibition trials, the 633nm laser is activated either during the sensory (texture) period or the delay period of the task. A masking LED is on for all trials, including no laser trials.

(**D**) Learning curves of an example mouse.

(**E**) A psychometric curve for no-laser trials in an example mouse. Textures are panels of black foil. The G5 texture has gratings made of P20 grit, G4: P150, G3: P220, G2: P1500, G1: foil strips, G0: foil only.

(**F**) Jaws-TdTomato expression in S1 layer 5 and POm of the example mouse from D with optic fiber implant in anterior-dorsal POm.

(**G**) Example electrophysiology recording in POm showing Jaws inhibition of S1 L5 to POm terminals in response to ChR2 activation from S1 layer 5. See **Suppl Fig. 2**.

(**H**) Example intrinsic signal optical (IS) imaging signal of C1 whisker stimulation through the cranial window of the example mouse from D (left). Jaws-TdTomato expression with overlaid S1 barrel map from IS imaging (middle). Barrels which did not localize with Jaws expression had their corresponding whiskers trimmed (Row A in example mouse from D) (right). Whiskers which did not contact the texture were left intact. Row E is not shown for clarity. wS2: whisker S2.

Inhibition of S1 layer 5 to POm terminals impairs discrimination performance. The effects of Jaws inhibition at S1 L5 to POm terminals on discrimination performance (**Fig. 2A**) were tested either during the texture presentation period of the task ("sensory laser") or during the delay period of the task ("delay laser"). The Jaws-activating 633nm laser measured 4 ± 0.2 mW at the tip of the implant (~127mW/mm^2). On trials without laser activation ("no-laser"), presentation of a range of textures with gratings revealed that mice were more likely to lick to the coarser gratings (G3-G5) and less likely to lick to the non-rewarded smooth texture (G0) (**Fig. 2B**, right, black curve). Sensory laser application resulted in a compressed psychometric function and a higher rate of errors (Miss and FA) (**Fig. 2B**). Psychometric parameters also reflected an increase in guess rates (false alarm) and lapse rates (miss) (**Fig. 2C**). The steepness of the psychometric curve (sensitivity) was reduced but the discrimination threshold (bias) was not shifted (**Fig. 2C**, right).

On separate days, the same mice were also tested on the effects of delay laser inhibition, which caused a shift of the psychometric curve to the right (**Fig. 2D**). There was a non-significant trend for the laser to increase error rate (**Fig. 2D**, bottom). Delay laser showed an expected increase in bias (threshold) but no effect on the slope of the curve (**Fig. 2E**). Laser inhibition also significantly increased lapse rate and guess rate. The inhibitory effect on performance was more subtle when applied during the delay epoch than during the sensory period.

To index performance, we calculated average d-prime for each grating texture compared to G0 texture (**Fig. 2F**). During no-laser trials, d-prime was higher for textures of coarser gratings compared to those of finer gratings. During sensory laser trials, d-prime was reduced for all textures. During delay laser trials, d-prime was reduced for the textures difficult to discriminate against G0 (G1, G2) but not significantly for the textures more easily discriminated (G3, G5). Overall, mice performed the best under no-laser conditions, could not perform without any whiskers, and showed impaired performance for inhibition during the sensory period (**Fig. 2G**).
Red light activation in the brain by itself can have effects on mouse behavior, since the light can activate retinal circuits (Danskin et al., 2015; Odoemene et al., 2018). One control for this was carried out as follows. In addition to Jaws-expressing mice, we tested mice that were injected with AAV carrying TdTomato without Jaws (n=4). These control mice did not show differences between no-laser and sensory laser trials for d-prime, error rate or psychometric curve parameters (**Suppl Fig. 3A, B**). The same TdTomato-expressing mice were also unaffected by laser application during the delay epoch of the task (**Suppl Fig. 3C, D**). The TdTomato control group showed that red laser delivery alone did not contribute to the behavioral effects seen in Jaws-expressing mice.

After finding different effects of sensory and delay laser applications, we tested both laser conditions within the same session using a subset of textures (G0, G1, G2, G5), in the same Jaws-expressing mice (n=9). Sensory laser was confirmed to increase error responses: we saw both increased misses to G5 (lapses) and increased false alarms to G0 (guesses) (**Fig. 2H**). Delay laser reduced lick response to texture G2 and G5, but there was no change to G0 responses. The more severe effect of laser application during the sensory period, compared to delay period, is supported by d-prime analyses (**Fig. 2F, I**). In addition to TdTomato controls, 3 of the 9 mice studied for effects of Jaws served as within-mouse controls for non-inhibitory effects of the red laser. An additional optic fiber was implanted subcortically, anterior to POm, away from Jaws-expressing terminals (**Fig. 2H**). When the laser was attached to the anterior control implant, there was no

effect of laser trials on performance (**Fig. 2H**). In further support of a Jaws-mediated effect, there was a positive correlation (r=.67, p=0.043, n=9 mice) between the errors made during sensory laser (guess and lapse rates) and proximity of the fiber implant to Jaws expression in POm (**Fig. 2J**).

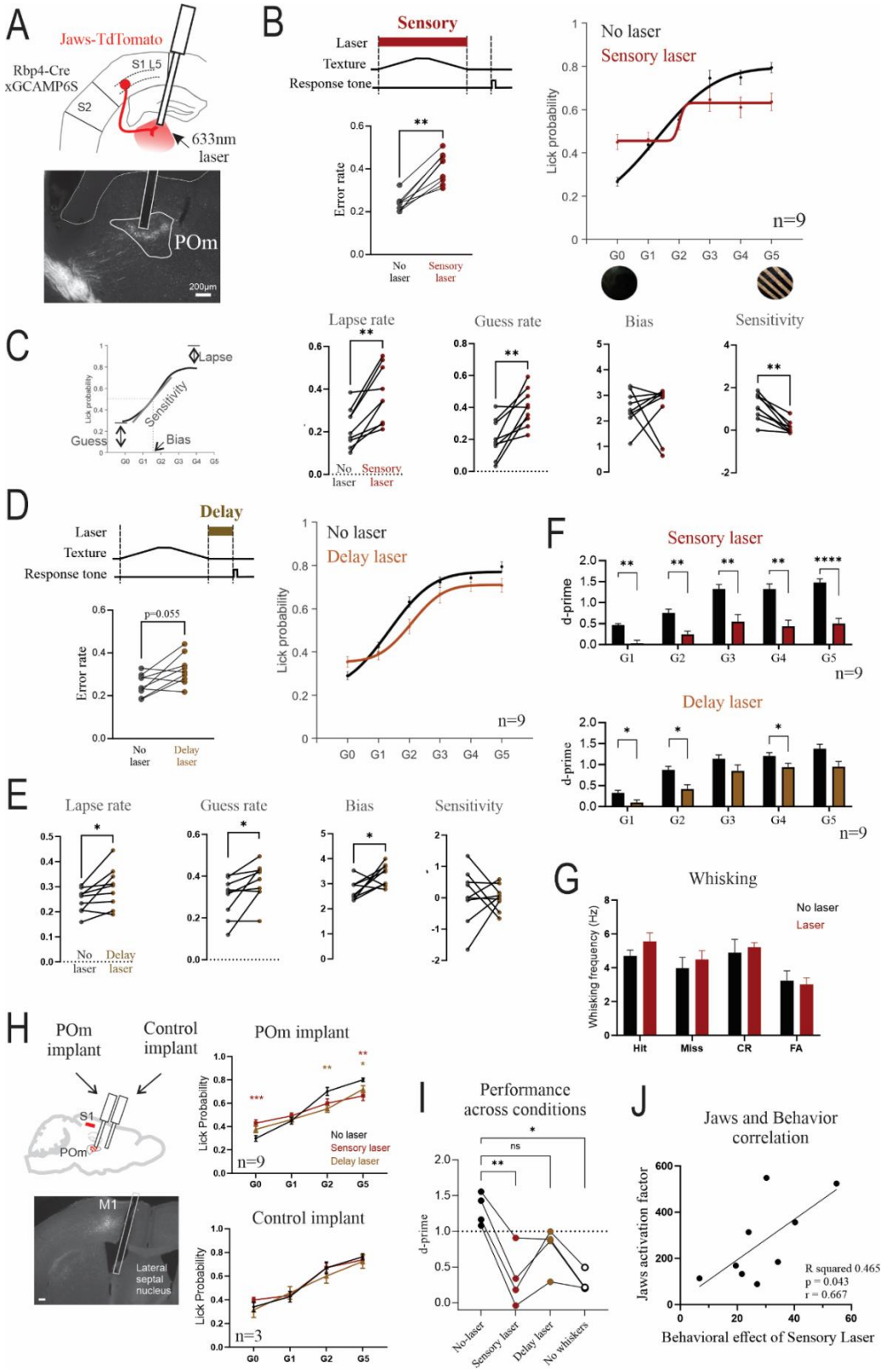

Figure 2. Inactivating the S1 L5 projection to POm impairs texture discrimination.
(**A**) Schematic of S1 L5 to POm terminal inhibition using Jaws opsin (top). Jaws-tdTomato expression and optic fiber implant in an example mouse (bottom).
(**B**) Schematic of sensory laser application during the texture presentation epoch of the task (top). Error rate for no-laser and sensory laser calculated from the average rate of Miss and FA trials, for G5 and G0 discrimination (n=9 mice) (bottom). No-laser vs sensory laser (mean ± sem): 0.23 ± 0.013 vs 0.41 ± 0.023, p=0.0039 (paired samples Wilcoxon test). The graph on the right shows curve fits for averaged data. Data points from individual mice (n=9) were an average of 4-9 sessions.
(**C**) Schematic of psychometric curve parameters (left). Parameters quantified from curves in **B** (right). No-laser vs sensory laser trials for lapse rate: p=0.0039, guess rate: p=0.0078, bias: p=0.82 and sensitivity: p=0.0039 (n=9 mice, paired samples Wilcoxon test).
(**D**) Schematic of delay laser application between the end of texture period and start of response epoch (top). Error rate (bottom) for no-laser and delay laser trials (p=0.055, paired samples Wilcoxon test). Psychometric performance with curve fits (right). Data are averaged from the same n=9 mice tested in sensory laser experiments (average of 4-9 sessions per mouse).
(**E**) Psychometric parameters quantified from curve in **D** (n=9 mice). No-laser vs sensory laser trials for lapse rate: p=0.027, guess rate: p=0.016, bias: p=0.039, sensitivity: p=0.91 (paired samples Wilcoxon test).
(**F**) D-prime performance across all textures for no-laser vs sensory laser (top, n=9 mice) for G1: p=0.0006, G2: p=0.0026, G3: p=0.0011, G4: p=0.0015, G5: p<0.0001 (two-way RM ANOVA, texture x laser interaction p=0.001, Bonferroni post-hoc tests). D-prime for no-laser vs delay laser (bottom, n=9 mice) for G1: p=0.023, G2: p=0.048, G3: p=0.10, G4: p=0.029, G5: p=0.11 (two-way RM ANOVA, effect of laser p=0.0011, texture x laser interaction p=0.36, Bonferroni post-hoc tests).
(**G**) Whisking analysis during the texture presentation epoch for no-laser and sensory laser trials (G5 and G0 trials, n=2 sessions from 1 mouse). Mixed-effects ANOVA, effect of laser p=0.391, effect of trial p=0.022, trial x laser p=0.784.
(**H**) Schematic of a second control implant targeting an area without Jaws expression (left, top). Example TdTomato fluorescence image of a control implant in the lateral septal nucleus of a Jaws-expressing mouse, scale bar=200μm (left, bottom). Sensory and delay laser testing within the same session for Jaws-expressing mice with laser attached to the implant in POm (top right, n=9 mice, averaged from 5-9 sessions per mouse). No-laser vs sensory laser for G5: p=0.0086, G0: p=0.0007. No-laser vs delay laser for G5: p=0.030, G2: p=0.0047, G0: p=0.150 (two-way RM ANOVA, texture x laser interaction p<0.0001, Bonferroni post-hoc tests). The same testing for mice when laser was attached to the control implant (bottom right, n=3 mice, averaged from 3 sessions per mouse). No effects or interactions found (two-way RM ANOVA).
(**I**) Averaged d-prime performance across trial conditions (n=4 mice, average of 3-9 sessions per mouse). No-laser vs Sensory: p= 0.0091, No-laser vs Delay: p=0.08, No-laser vs No-whisker: p=0.021 (one-way RM ANOVA, p=0.0056, Bonferroni post-hoc tests).
(**J**) A plot of the relationship between the behavioral effect of Sensory laser (Guess rate (No laser – Laser) + Lapse rate (No laser – Laser)) and estimation of Jaws terminal activation (expression area and distance from the optic fiber implant). R-squared=0.46, r=.67, F=6.07, p=0.043.
Values shown as mean ± standard error of the mean. * p<0.05, ** p<0.01, ***p<0.001.

A potential explanation for the impaired ability to discriminate textures during S1 L5 to POm terminal inhibition could be reduced sampling of the textures, that is, reduced whisking of the textures, although this would not apply to the delay laser data. However, whisker analysis during the sensory period did not show differences in number of whisks between no-laser and sensory laser trials (**Fig. 2G**). A motor-mediated explanation of impaired performance is thus unlikely.

Performance on a Detection Task

In contrast to discrimination, the ability to detect a whisker-based stimulus has been shown to be independent of S1 (Hong et al., 2018, Park et al., 2022) and thus independent of the S1 L5 transthalamic projection. We tested this hypothesis with the same Jaws-mediated inhibition on a detection task analogous in design to our discrimination task (**Fig. 3A**). Instead of a whisker deflection task with overlapping stimulus and response windows (Takahashi et al., 2016; Yang et al., 2016; Le Merre et al., 2018; Takahashi et al., 2020), we used a movement detection task where mice must detect the deflection of a panel sitting in their whisker field, followed by a 1 second delay before a response cue (**Fig. 3B**). Catch trials of no-movement were presented to test for conditioned licking to the response cue. We trained 4 Jaws-injected mice in the detection task, 3 of which also learnt the discrimination task. Inhibition of the S1 L5 to POm projection shifted the psychometric curve to the right (**Fig. 3C**), increasing the threshold of detection but not affecting sensitivity, lapse and guess rates (**Fig. 3D**). Controls consisted of TdTomato-injected mice (n=3, 1 from discrimination task) and Jaws-injected mice with the laser attached to a second optic fiber implant, as described in the discrimination task (n=2) (**Fig. 2H**). Detection performance in these control mice were no different on laser trials (**Fig. 3E, F**). The impaired detection performance corroborates with a study that used inhibitory DREADDs to suppress the projection (Takahashi et al., 2020). However, in contrast to Takahashi et al., we did not find a reduction in response to no-movement catch trials (**Fig. 3C**). This is perhaps because optogenetics can be selectively applied to the sensory and delay epochs, avoiding inhibition during the response period.

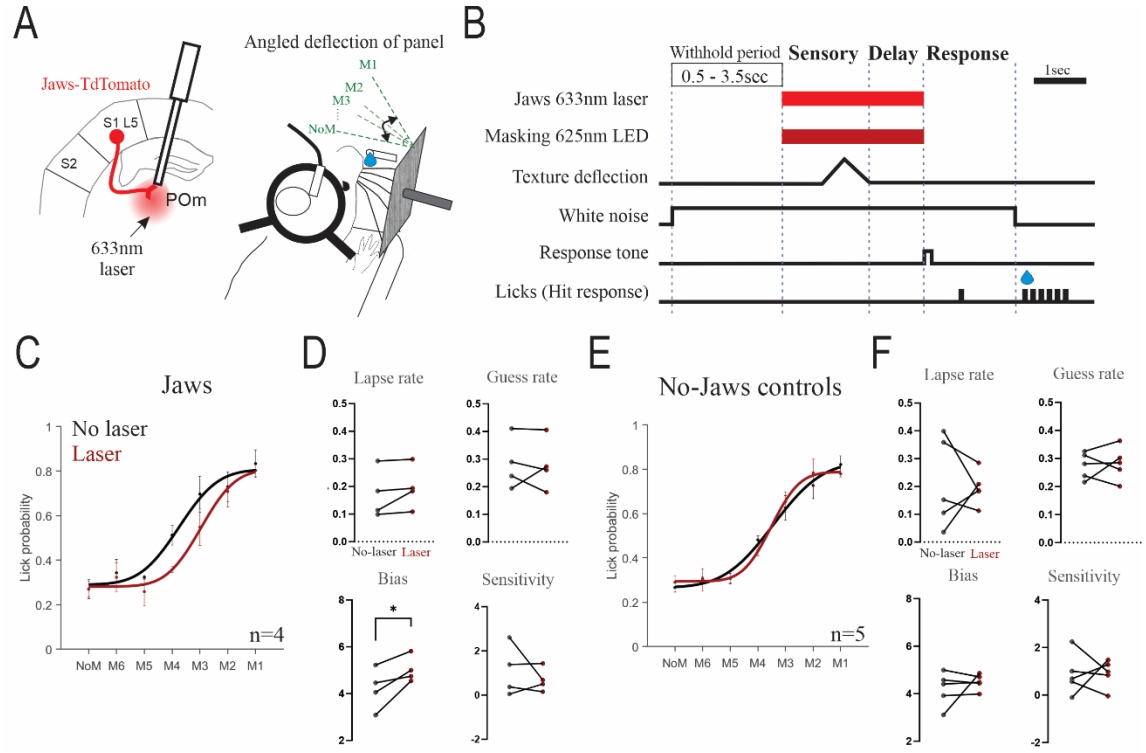

Figure 3. Inhibiting the S1 L5 projection to POm impairs whisker-based detection

(**A**) The S1 L5 to POm projection was targeted for inhibition at the terminals by the Jaws opsin in Rbp4-Cre mice. Mice were trained to lick at angled movements of a panel located within their whisker field (Hit) and withhold licking to no-movement (NoM) (correct rejection).

(**B**) Time course of a Hit trial. A variable pre-movement period reduced prediction of the movement, white noise masked auditory cues and a 625nm LED on every trial habituated the retina to red light. Movement angles M1 – M6 corresponded to 20.5, 13.7, 6.9, 3.4, 1.7, 0.89°.

(**C**) Psychometric fits for performance in mice with Jaws expression (n=4 mice, 3 also learnt the discrimination task). Datapoints for each mouse are an average of 4-6 sessions.

(**D**) Psychometric parameters for the curves in **C**. No-laser vs laser comparisons for lapse rate: p=0.22, guess rate: p=0.91, bias: p=0.048 and sensitivity: p=0.49 (paired t-tests).

(**E, F**) Same as **C** and **D** for no-Jaws control mice (n=5: 3 TdTomato-expressing mice, 1 of which also learnt the discrimination task, and 2 Jaws mice with control optic fiber implants, which also learnt discrimination). Datapoints for each mouse are an average of 3-6 sessions. No-laser vs laser comparisons for lapse rate: p=0.38, guess rate: p=0.60, bias: p=0.39 and sensitivity: p=0.52 (paired t-tests). Error bars show standard error of the mean. * p<0.05.

EFFECTS OF SUPPRESSING THE TRANSTHALAMIC PATHWAY ON CORTICAL RESPONSES

We focus our cortical cell analyses on the discrimination task, the behavior during which we saw the largest effect of transthalamic inhibition (**Fig. 2**). Very few cells showed responses specific to the delay period of the task (data not shown), so further analysis is restricted to comparing no-laser and sensory laser trials.

The behavioral impairment resulting from inhibition of S1 L5 to POm terminals could affect encoding in any areas targeted by POm involved in texture discrimination, notably S1 and S2 (Chen et al., 2015; Gilad et al., 2018; Chéreau et al., 2020; Gilad and Helmchen, 2020; Gallero-Salas et al., 2021). To investigate this, we imaged single cell calcium activity via GCAMP6S in layers 2/3 of S1 and S2 in 5 of the 9 Jaws-expressing mice used in the behavioral experiments (**Fig. 4A**).

We quantified texture responsiveness by measuring area under the curve (AUC) of the calcium transient ($\Delta F/F$), and a response was defined as the AUC during the sensory period minus that of the baseline period (**Fig. 4B**). In contrast to corticocortical silencing, which affects both direct and transthalamic pathways and reduces overall population responsiveness to a sensory stimulus (Nurminen et al., 2018; Javadzadeh and Hofer, 2022), inhibiting the transthalamic pathway did not reduce activity to texture presentation per se (**Fig. 4B**). During no-laser trials, cells in both S1 and S2 showed higher texture responses on G5 hit trials compared to G0 CR trials (**Fig. 4B, E**) in accordance with previous studies on texture discrimination (Chen et al., 2015; Gilad et al., 2018; Chéreau et al., 2020; Gilad and Helmchen, 2020). S1 L5 to POm terminal inhibition during the sensory period did not affect this preference for the G5 rewarded texture in S1 but disrupted the discrimination in S2 (**Fig. 4B, C**). The responsiveness of S2 cells to the texture (hit trials) also correlated with the effect of the laser, as measured by laser-induced change in texture responsiveness. This relationship was not seen in S1 cells (**Fig. 4D**).

These data suggest that the transthalamic pathway disrupts the differential response to texture stimuli in S2, which aligns with disrupted behavioral performance. To further quantify stimulus selectivity, we used receiver-operating characteristic (ROC) curve analysis to calculate a Discrimination Index (DI) for each cell, which expresses the likelihood that an ideal observer correctly classifies trial type (i.e. hit texture vs CR texture), based on the dF/F during the sensory period (**Fig. 4F**) (Chéreau et al., 2020; Gilad and Helmchen, 2020). A permutation test was used to determine if the DI was statistically significant. A positive DI represents selectivity (larger response) for the G5 Hit texture and a negative DI represents selectivity for the G0 CR texture. In mice proficient in the discrimination task, the proportion of cells with significant DI (positive or negative) were no different during no-laser and laser conditions, in S1 or S2 (**Fig. 4F)**. However, there was a higher fraction of cells selective for the hit texture compared to the CR texture, in both S1 and S2, and laser inhibition disrupted this selectivity in S2, whilst non-significantly in S1 ($p=0.051$, no-laser vs laser G5 selective fraction) (**Fig. 4G, H**). We have thus shown using two different analyses (AUC texture responsiveness and ROC analysis) that sensory laser application reduces selectivity in the S1 population and acts to reverse texture selectivity towards the unrewarded G0 texture in the S2 cell population.

Are the populations of discriminating cells different during no-laser and laser stimulation? We investigated each significant DI cell under the two laser conditions and found that 100% of S2 cells did not discriminate in the other laser condition and 94% of S1 cells also showed non-significant DI once the laser was on or off (**Fig. 4I**). Thus, no cells with significant DI switch selectivity for Hit or CR textures during the laser application. This suggests that entirely separate populations of discriminating cells are recruited during laser inhibition, in S1 and S2.

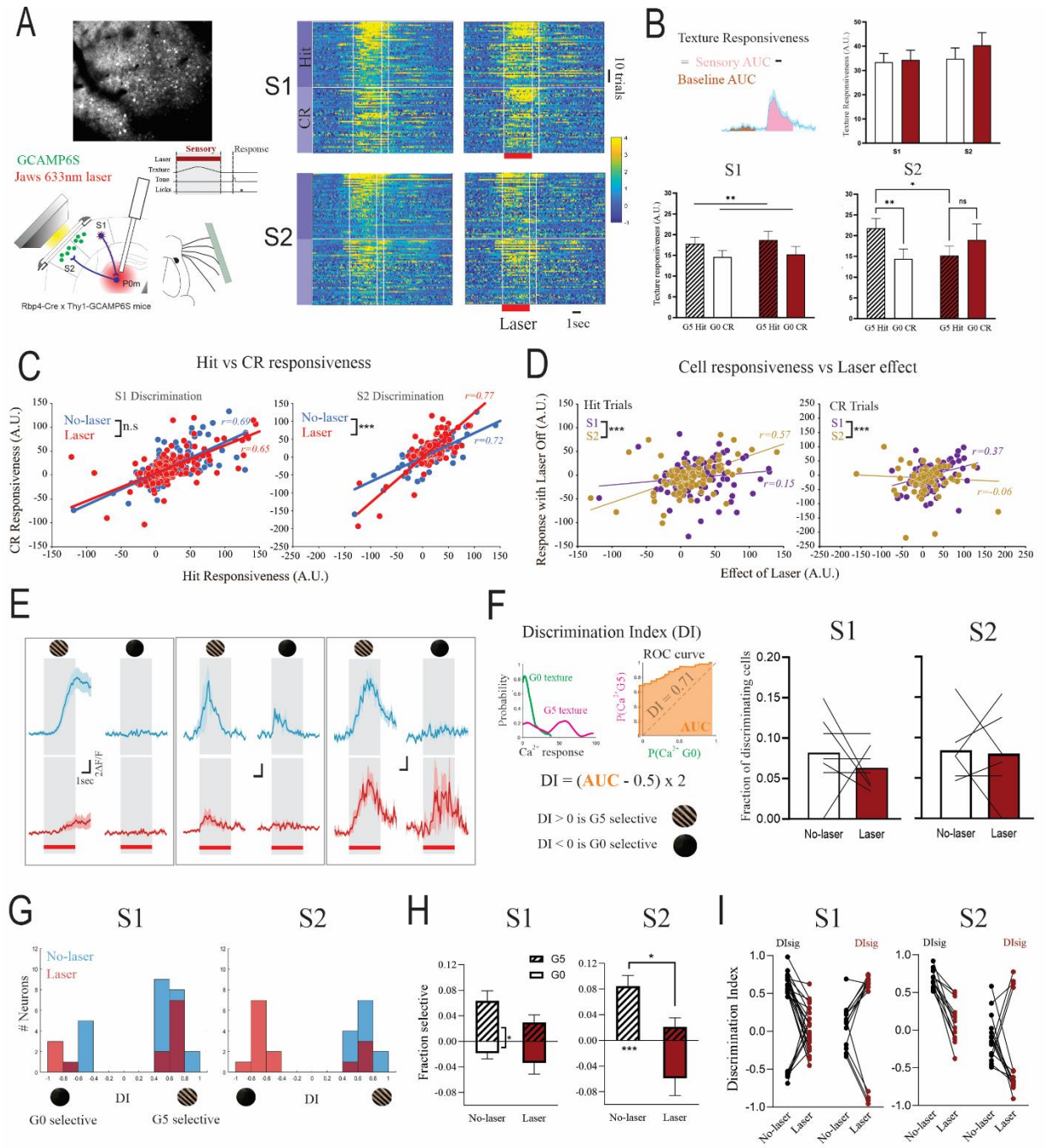

Figure 4. Inhibiting the transthalamic pathway disrupts discriminability of S2 cells with smaller effects on S1 cells.

(**A**) Schematic of concurrent calcium imaging and inhibitory optogenetics during texture discrimination (left). Heatmaps of texture-responsive cells during Hit and CR trials, in S1 and S2 (right). (**B**) Texture responsiveness value calculation (AUC for texture period - AUC for baseline period) (top left). Absolute value of texture responsiveness averaged across trial types (hit, miss, CR, FA) for no-laser and laser conditions (top right) (two-way ANOVA, effect of laser p=0.1155). Texture responsiveness for hit and CR trials for no-laser and laser conditions in S1 (bottom left) and S2 (bottom right). For cells with negative responsiveness values during no-laser hit trials, value signs were reversed across trial types. S1: two-way RM ANOVA, effect of texture p=0.0033, n=240 cells from 7 experiments in 4 mice. S2: two-way RM ANOVA, effect of texture p=0.64, effect of laser p= 0.31, laser x texture p=0.0002, no-laser hit vs CR p=0.0013, no-laser hit vs laser hit p=0.032, laser hit vs CR p=0.86 (Bonferroni post-hoc test), n=158 cells from 6 experiments in 3 mice.

(**C**) Scatterplot of texture responsiveness values for hit vs CR trials in S1 (left) and S2 (right). S1 no-laser vs laser slopes p=0.24 (n=240 cells), S2 no-laser vs laser slopes p<0.0001 (n=158 cells). Pearson correlations (r) are shown.

(**D**) Effect of laser (Texture responsiveness for no-laser – laser) vs hit responsiveness (no-laser trials) in S1 (left) and S2 (right). S1 no-laser vs laser slopes p<0.0001 (n=240 cells), S2 no-laser vs laser slopes p<0.0001 (n=158 cells). Pearson correlations (r) are shown.

(**E**) Normalized calcium transients for example cells in response to the rewarded texture (G5, left) compared to the unrewarded texture (G0, right) for no-laser trials (top row) and laser trials (bottom row). S2 cells: left and middle, S1 cell: right. Grey shading represents texture presentation period.

(**F**) Discrimination index (DI) calculation based on ROC analysis, where positive DI represents G5 texture selectivity and negative DI represents G0 selectivity (left). Statistical significance was determined using a permutation test. Fraction of significant DI cells for no-laser and laser trials, in S1 (7 experiments, p=0.62) and S2 (6 experiments, p=0.75, Wilcoxon test) (right).

(**G**) Distribution of G5 and G0 -selective DIs during no-laser and laser trials, for S1 and S2. (**H**) Fraction of cells with significant DIs selective for the G5 and G0 textures for no-laser and laser trials, in S1 and S2. S1: no-laser G5 vs no-laser G0 p=0.0164, laser G5 vs laser G0 p=0.27 (McNemar's test), no-laser G5 vs laser G5 p=0.051 (z-test). S2: no-laser G5 vs no-laser G0 p=0.0009, laser G5 vs laser G0 p=0.18 (McNemar's test), no-laser G5 vs laser G5 p=0.025 and no-laser G0 vs laser G0 p=0.0013 (z-test).

(**I**) For S1 (left) and S2 (right), significant DIs were plotted for no-laser (left column) and laser (right column) trials, with their corresponding DIs during laser and no-laser trials, respectively.

Values shown as mean ± standard error of the mean. * p<0.05, ** p<0.01, *** p<0.001.

DISCUSSION

Recent evidence suggests that cortico-thalamo-cortical pathways through higher order thalamus are distinct and influential routes of sensory processing, compared to direct corticocortical projections (Blot et al., 2021), but many details of their contribution are unknown. To study this further, we inhibited the somatosensory transthalamic pathway at the terminals of S1 L5 to POm and found that this had deleterious effects on the ability of the mouse to sense objects by whisking. These perceptual errors coincided with impaired stimulus selectivity of neurons in S2 and to a lesser extent in S1, suggesting a new role of cortico-thalamo-cortical pathways in sensory choice. These causative results extend previous work on the neural basis of texture discrimination and cortical information flow for perceptual decisions.

BEHAVIORAL EFFECTS

The design of our behavioral task allowed us to distinguish effects of inhibiting the transthalamic pathway(s) separately during the sensory sampling period and during a delay period (**Fig. 1)**, rather than silencing throughout the entire behavioral trial (Chen et al., 2013; Takahashi et al., 2020; Park et al., 2022; Qi et al., 2022). We report discrimination deficits due to the inhibition during both periods, albeit to a lesser degree during the delay epoch.

During the sensory period

Inhibition during texture presentation severely impaired discrimination performance, increasing total errors, lapse rates and guess rates (**Fig. 2B, C**). This is also likely an *underestimate* of the effects of S1 L5 to POm terminal inhibition, because complete efficiency of Jaws expression in S1 L5 to POm terminals is not feasible, and precisely-targeted probe placements are required for strong behavioral and imaging effects (**Fig. 2H**).

We found deficits due to inhibition of the transthalamic pathway not only on somatosensory discrimination but also on detection (**Fig. 3**). Evidence exists that whisker-based detection can occur in the absence of barrel cortex (Hong et al., 2018; Park et al., 2022) and thus presumably in the absence of the S1 L5 to POm projection. However, others have found that suppressing the S1 L5 projection to POm using chemogenetics impairs tactile detection . Our results suggest that such inhibition impairs performance by increasing the threshold to detect a small movement but does not alter detection of larger ones (**Fig. 3C, D**). Thus, the S1 L5 to POm projection affects detection thresholds rather than detection per se.

During the delay period

The behavioral impairment during inhibition of the delay period suggests that transthalamic signaling is ongoing after sensory sampling and contributes to task performance. Interestingly, persistent activity in cortical areas rely on constant input from higher order thalamus for processes such as working memory and premotor planning (Reinhold et al., 2015; Bolkan et al., 2017; Guo et al., 2017). It is thus plausible that inhibition of S1 L5 transthalamic processing reduces thalamic input to cortical regions and potential cortical targets from POm include association cortices such

as M2 (Gilad et al., 2018; Gallero-Salas et al., 2021), which has an S1 L5 transthalamic input (Mo and Sherman, 2019). Other brain regions innervated by transthalamic pathways from S1 could also play a role in our behavioral effects.

By restricting inhibition to the sensory or delay epochs of the task, we avoided any potential confounds of suppressing the ability to report the sensory choice. We also confirmed that optogenetic inhibition did not affect the amount of whisking (i.e. sensory sampling) (**Fig. 2K**), and during the detection task, inhibition did not induce perceived whisker movements during catch trials (**Fig. 3C**). It is thus unlikely that reduced or aberrant motor activity can explain the impaired behavioral performance.

Effects on Neuronal Responses

We conclude from the behavioral data that the transthalamic pathway is crucial for somatosensory discrimination, particularly during the stimulus sampling period. What information is the pathway propagating during this sensory period that is necessary for performance?

We investigated this question using 2-photon calcium imaging and concurrent optogenetic inhibition in a subset of the same mice that underwent behavioral testing. In agreement with previous studies, during texture discrimination performance, cells in S1 and S2 show Hit/CR discrimination: calcium activity in response to textures during Hit trials is higher compared to correct rejection trials (Chen et al., 2013; Chen et al., 2016; Gilad et al., 2018; Gallero-Salas et al., 2021). This selectivity for the hit texture over the unrewarded CR texture is a key correlate of expert discrimination performance and successful reversal learning (Chen et al., 2015; Chéreau et al., 2020; Gilad and Helmchen, 2020). We now show causal evidence that the stimulus texture selectivity is a neural substrate of correct discrimination. Inhibition of the transthalamic projection abolished hit selectivity of the S1 and S2 populations (**Fig. 4B, C, G, H**), in alignment with increased performance errors (**Fig. 2B**). However, inhibition did not change the total proportion of texture discriminating cells (**Fig. 4F**). Instead, it changed the relative proportions of cells selective for either the hit and CR texture in S1 and S2 (**Fig. 4G, H**). In the absence of signaling via the somatosensory transthalamic activity, S1 and S2 cells that normally showed discriminability, no longer differentially responded to the textures. In a subset of cells that were not previously discriminating, stimulus selectivity was induced (**Fig. 4I**). In S1, the cells that gained discriminability during transthalamic inhibition, were equal fractions of those selective for the hit and CR textures (**Fig. 4H**). This equal fraction of hit vs CR selective cells is also found in naïve mice who have not yet learned the task (Chéreau et al., 2020; Gilad and Helmchen, 2020). In S2 however, inhibition induced more cells to be selective for the CR texture compared to hit texture (**Fig. 4H**), causing a reversal of S2 population texture selectivity. Without a population preference for the salient, behaviorally-relevant reward stimulus, behavioral performance is no longer supported.

How could inhibiting the transthalamic pathway cause such a disruption of cellular discriminability? During multiple days of initial task learning or reversal learning, mechanisms of plasticity and reorganization of connectivity have been implicated in supporting changes in discriminability (Banerjee et al., 2020; Chéreau et al., 2020; Poort et al., 2022). However, optogenetic inhibition occurs on a trial-by-trial basis and the effect of inhibition on population

discriminability may be better explained by top-down modulation over shorter timescales (Poort et al., 2022). For example, stimulus discriminability may depend on integrating sensory and reward inputs in S1 and carried by its L5 outputs. Indeed, reward signals have been demonstrated in the dendrites of S1 L5 cells (Lacefield et al., 2019), the inhibition of which blocks reward-based learning (Schoenfeld et al., 2022). Thus, the transthalamic pathway may deliver trial-by-trial information on the salience of stimuli to POm for subsequent propagation to S1 and higher order cortex. The signaling via POm may allow integration with, and inhibitory control of, subcortical inputs (Trageser and Keller, 2004; Lavallée et al., 2005; Groh et al., 2014). The present results and other evidence for the influence of corticothalamic projections (Musall et al., 2023) suggest that transthalamic pathways play a powerful role in perception.

CONCLUSIONS

In summary, we have presented behavioral and neuronal data that causally implicate the transthalamic pathway in propagating stimulus feature selectivity for correct perceptual decisions. Our results demonstrate the need to include transthalamic circuits and higher order thalamus in the framework for cortical functioning.

METHODS

ANIMALS

All experiments were performed in accordance with protocols approved by the Institutional Animal Care and Use Committee at the University of Chicago. Transgenic mice expressing Cre-recombinase in layer 5 of cortex (Rbp4-Cre) (Gerfen et al., 2013) were bred by crossing hemizygous male Tg(Rbp4-cre) KL100GSat/Mmcd mice (GENSAT RP24-285K21) with female C57Black6J mice. Rbp4-Cre positive offspring were used for *in vivo* electrophysiology experiments (**Fig. 1G**, **Suppl. Fig. 2**). All other data were generated with Rbp4-Cre x Thy1-GCAMP6S mice, created by breeding male Rbp4-Cre mice with female Thy1-GCaMP6S mice (GP4.12Dkim/J, Stock: 025776, The Jackson Laboratory). Tail biopsies were taken at 14-21 days old and genotyped by real time polymerase chain reaction (Transnetyx, Cordova, TN). Mice used in behavioral experiments were a balanced mix of male and female and housed individually on a reverse light-dark cycle (7am-7pm) after their first surgery. Behavioral training and testing were performed in the animal's active dark cycle. All mice were given food and water *ad libitum*, unless water restricted as described (see **Behavioral set up and discrimination task**).

SURGICAL PROCEDURES

Mice were anaesthetized with a ketamine (100 mg/kg)/xylazine (3 mg/kg, i.p) cocktail and maintained on isoflurane (1.0-1.5% in oxygen). Using aseptic technique, a small burr hole was made over the target site and virus was injected using a 0.5uL syringe (7000.5KH, Hamilton, Reno, NV) at a rate of 5-10nl/min. To express Jaws-TdTomato or TdTomato alone in layer 5 of S1, we injected 350nl of AAV8-CAG-FLEX-Jaws-KGC-TdTomato-ER2 (UNC Vector Core) or AAV5-CAG-FLEX-TdTomato (UNC Vector Core) into left S1 of 6 week old Rbp4-Cre or Rbp4-Cre x

GCaMP6S mice. Left hemisphere S1 coordinates relative to bregma were DV: −0.5, ML: 3.1mm, AP: -0.8mm. After 2 weeks, a custom titanium head post (11.5mm diameter, H.E. Parmer) was adhered to the skull using dental cement (C&B Metabond). To ensure firm adherence, the left temporal muscles were retracted and the exposed skull was dried and lightly scored using the drill. In the same surgery, a cranial window was implanted over S1 and S2 (DV: −0.5, ML: 4.1mm, AP: -0.7mm). The window was a 4mm diameter glass circle (0.66mm thick, Tower Optical) attached to a glass coverslip (5mm diameter, CS-5R, Cat. 64-0700, Warner Instruments) using an optically clear ultraviolet curing adhesive (Norland Optical). An optic fiber stub (200µm diameter, .5NA, Thorlabs) was also implanted at 8° from the vertical to target left POm (DV: -3.1mm, ML: 1.2mm, AP: -0.6mm). In some mice, a second optic fiber was implanted subcortically, anterior to POm. After all surgeries, animals were treated locally with lidocaine hydrochloride (Akorn, Buffalo Grove, IL) and vetropolycin antibiotic ointment (Dechra, Overland Park, KS). Analgesia (Meloxicam, 1-2mg/kg, s.c) was administered pre-operatively and 24 hours post-operatively.

Intrinsic Signal Optical Imaging

To confirm that the expression of Jaws was restricted to S1, we functionally located S1 and S2 in each mouse using intrinsic signal optical (IS) imaging. IS imaging allows the visualization of hemodynamic changes due to cortical activity, such as that induced by whisker stimulation. One week after window and implant surgery, mice were induced with 3% isoflurane in oxygen and maintained on 1%, during which body temperature and breathing rate was monitored. Reflected light through the cortical window was imaged using a CCD camera (Teledyne QImaging, Retiga-SRV). The surface vasculature was visualized under green illumination (525nm) and hemodynamic response was captured under red illumination (625 nm). Multi-whisker responses were stimulated with a textured panel, 2cm away from, and perpendicular to, the whisker pad. The texture was moved at 3Hz in the anteroposterior direction. Single whisker responses in cortex were stimulated by moving single whiskers, threaded by a pipette tip, at 5Hz in the anteroposterior direction. Image acquisition onset was 1 second after stimulus application (4 second duration). Custom-written MATLAB code recorded 3 seconds of activity on each trial, alternating between no-stimulation trials and stimulation trials (30 trials each, 8 seconds inter-trial interval). The signal was quantified as the difference in the reflected light during the stimulus trials and no-stimulus trials.

Trimming so task-relevant whiskers and Jaws-expressing S1 barrels

For each mouse, the whisker map generated from IS imaging was overlaid with the fluorescence image of Jaws-TdTomato. If the S1 barrels of task-relevant whiskers did not express Jaws-TdTomato, the corresponding whiskers were trimmed down to the whisker pad (**Fig. 1H**). Task-relevant whiskers were verified for each mouse as those which consistently came into contact with the texture panel during the discrimination task (typically alpha, A1, beta, B1, B2, gamma, C1, C2, delta, D1, and D2 whiskers). Whisker length was monitored every 3-4 days and re-trimmed as necessary.

Behavioral Setup and Discrimination Task

Set up

The behavioral enclosure was light-proof and fitted with soundproof panels (0.8 NRC, Sound Seal) with the following internal light sources: An infrared webcam (webcamera_usb) with its LEDs shielded with Kimwipe tissue, and a 625nm LED (Thorlabs) with the output diffused with an acrylic panel and Kimwipe tissues. The 625nm LED was positioned 20cm in front of the mouse's face and emitted during the sensory period of every trial. Speakers delivering the response tone (8kHz, MATLAB) were positioned such that the sound level was 60dB at the distance of the mouse. A pump (NE-1000 syringe pump, New Era) delivered water through a spout (15G blunt needle) mounted 3-6mm away from the mouth. Licks were detected by a capacitance sensor attached to the spout (Teensy 3.2, PJRC). Mice were able to run freely on a custom-built treadmill. Textured panels (5.5cm diameter circles) were attached to a custom-built 8-sided wheel (7cm radius), rotated by a stepper motor (X-NMS17C, Zaber). Textures were presented one at a time to the mouse by mounting the stepper motor vertically on a linear slider (X-LSM050, Zaber) and advancing it into, and retracting it out of, the right whisker field. At the start of each trial, the wheel was rotated in either direction for a random amount of time (0.34 - 1.8 seconds) to prevent predictive auditory cues. From this position, the wheel moved to the texture panel selected for the trial and the linear slider advanced the texture from 3.7cm from the whisker pad, to 2.2cm away, still out of reach of most whiskers, and then into the whisker field, 1.2cm away from the pad. The texture was held at this position for 0.5 seconds and retracted out of reach of the whiskers, upon which there was a delay period (0.6-1 seconds), followed by the tone and response period. Synchronization and triggers were controlled through MATLAB (2020b).

Habituation

One week after window surgery, mice were water restricted to 80-95% weight and habituated to the head-fix apparatus within the enclosure over 3-5 days. During the habituation period, mice were first encouraged to lick the spout (8uL water delivery). Then, water delivery was paired with a preceding tone (8kHz) until mice self-triggered the delivery by licking the spout within 2 seconds of the tone onset.

G5 and G0 discrimination training

Mice were then trained on a go/no-go design to discriminate between a smooth texture (no-go: matte, black, aluminum foil) and one with a grating (go: gratings on foil). The grating textures were made of 5mm-wide sandpaper strips, 7mm apart on black foil. During initial training, the presentation of a grating texture (P20 grit strips: G5 texture) was associated with a water reward (6uL). For the first few trials of G5 presentation, water delivery was triggered immediately after the response tone. Then, water was only delivered if mice licked the spout after the tone, but within the response period (1.8 seconds). Water delivery only occurred after the end of the response period. Licking during the delay period triggered one alarm beep (NE-1000 syringe pump, New Era), aborting the trial for immediate restart. Licking during the response period of a G5 trial, the trial was deemed a "hit". No-lick response to the G5 texture during the response period was regarded a "miss". If the mouse performed 3 hit trials in a row, then the no-go G0 texture was introduced. Licking during the response period to the G0 texture triggered a beeping alarm (65dB,

NE-1000 syringe pump) and 12 second timeout ("false alarm", FA). If mice correctly withheld a lick response to the G0 texture, this was a "correct rejection" (CR) and punishment was avoided. If the previous two G0 textures were FAs, a mild air puff to the snout region was also administered (Cleaning duster, Office Depot). The consequence for a miss and CR response was moving to the next trial. G5 and G0 textures were presented in random order but with not more than 2 in a row and the inter-trial interval was 3-5 seconds. During G5 and G0 discrimination training, the delay period was 0.6 seconds, and gradually extended to 1 second. The response period was shortened from 2 to 1.6 seconds within the first week of training. Mice were considered trained when performance reached a d-prime of >1 or >70% correct for two consecutive days, which typically required 1-5 weeks. On training and testing days, mice were allowed to perform the task until sated and then supplemented in their home cage with 0-0.8ml water to maintain a body weight of 80-95%.

Psychometric and laser testing

After learning to discriminate G5 and G0, textures of various coarseness were presented in randomized order (G4=P100, G3=P220, G2=P1500, G1=foil strips on foil) in addition to G5 and G0. G0 was presented on 30% of trials. Effects of the laser (see **Optogenetic inhibition**) were initially tested during two conditions, in separate testing sessions on alternate days: 1) laser during the sensory period (3.8 seconds) 2) laser during the delay period (1 second). For each session, laser and no laser trials were presented at 50% each, except when the mouse was returned to G0 and G5 training (see **Bias correction**). In a third testing condition, both sensory laser trials and delay laser trials were tested in the same session but only textures G0, G1, G2 and G5 were presented. This testing was used during 2-photon imaging. Behavioral sessions were run daily and typically consisted of 150–400 trials lasting between 1 - 2 hours. Only sessions during which mice performed for no-laser trials (d-prime>1 or >70% correct) were included in the analyses.

Bias correction

To combat the high bias towards go responses during the beginning of each session (Berditchevskaia et al., 2016), mice are only minimally water restricted were possible (80-95%) and given "warm-up" training on G5 vs G0 discrimination. To proceed to psychometric testing, mice must respond to randomized G0 presentations with three CRs in a row (no FAs), which typically required 7-150 trials. Mice are returned to G5 vs G0 training if they perseverate (lick at every trial) or disengage (no lick response) on a sliding window of 7 trials. Any G5 v G0 bias correction trials were excluded from analyses.

Behavioral analyses

Correct performance was calculated for each session from G5 and G0 trials, by the formula:

$$(\text{hit trials} + \text{CR trials}) / (\text{hit} + \text{CR} + \text{miss} + \text{FA trials}) \times 100$$

D-prime was calculated by the difference in z transforms of G5 hit rate and FA rate:

$$d' = z(hit) - z(FA)$$

Error rate was calculated by taking the average of mean miss trials during G5 presentation and mean FA trials. For each laser testing condition in each mouse, psychometric curves were fitted with a 4-parameter sigmoidal cumulative gaussian function (Wichmann and Hill, 2001):

$$y(x) = g + (1 – g - l) * 0.5 * (1 + erf((x - u)/sqrt(2*v^2)))$$

where y(x) is the lick probability, x is the texture and erf represents the error function. The parameters to be fitted are: g (guess rate), l (lapse rate), u (subject bias), and v (discrimination sensitivity).

To plot the relationship between the behavioral effect and Jaws expression (**Fig. 2J**), the difference between the guess and lapse rates during no-laser and sensory laser trials was plotted against the estimation of Jaws terminal activation. A terminal activation factor was calculated by the area of Jaws terminal expression in POm, multiplied by the distance between the end of the implant and the middle of the expression site, for anatomical section with the deepest implant.

Optogenetic Inhibition

Optic fiber implants (200µm diameter, .5NA, Thorlabs, see Surgical procedures) were attached to a patch cable (0.5NA, Plexon) to deliver a 633nm laser (LuxX 633-100, Omicron-Laserage) with an estimated power output of 4 ± 0.2 mW. To reduce fluorescence artefacts of the laser during 2-photon imaging, autofluorescence from the patch cable was removed by photobleaching overnight using a 620nm LED (PlexBright, Plexon, 3.5-5mW at tip). During imaging, the red channel photomultiplier tube (PMT) was shuttered closed.

Whisker Tracking

Whisker movements were recorded from above using a CMOS high-speed camera at 122fps (Basler acA800-510um). The whiskers were illuminated with light from an IR camera and white cardboard provided background contrast. However, light levels were not increased for optimal tracking to avoid interfering with concurrent calcium imaging. Thus, whiskers could only be successfully tracked for a subset of sessions. We used custom Matlab code to run a convolutional neural network to label whiskers and a hough transform to extract whisker positions and angles. Analysis was restricted to movements from multiple rows of whiskers within 2cm of the whisker pad during the texture presentation period of the task for G5 (hit and miss) and G0 (CR and FA) trials. A whisk was defined as a continuous sweep > 25 pixels in the antero-posterior axis. The rate of whisking was calculated by the number of whisks / sensory period (3.84 seconds).

Detection Task

In the same behavioral set up as the discrimination task, mice were trained to detect the movement of a textured panel (P20 sandpaper) positioned within the whisker field (1.5cm from the whisker pad). The panel was mounted to the same texture wheel driven by the stepper motor

(X-NMS17C, Zaber) used in the discrimination task. The panel was deflected anteriorly and immediately returned its original position.

The task followed a go no-go task design, but here the panel movement was the go rewarded cue and no-movement was the no-go punished cue. To minimize timed prediction of a movement, a randomized "withhold" period of 0.5 – 3.5 seconds preceded the deflection. If mice licked during this period, an alarm beep would sound (NE-1000 syringe pump, New Era) and the trial was aborted and restarted. White noise (Matlab) throughout the trial masked auditory cues from the stepper motor. There was a 1 second delay after the sensory period (panel movement) but before the response tone (8kHz). Licks during the delay period also aborted the trial for restart. Mice are free to move on a treadmill.

Mice were first trained to lick to the largest movement (M1: 20.5°) compared to no-movement (NoM: 0°) and considered trained when performance reached d-prime of >1 or >70% correct for two consecutive days. This typically required 3-7 days. Psychometric and laser testing was then conducted with a range of angles: M2 – M6 corresponding to 13.7, 6.9, 3.4, 1.7, 0.89°. A 625nm LED was emitted during the sensory and delay periods of every trial. The 633nm laser was applied throughout the sensory and delay periods of the task. Behavioral analyses followed that of the discrimination task.

TWO-PHOTON CALCIUM IMAGING

GCAMP6S activity from Rbp4-Cre x Thy1-GCAMP6S mice was excited through a 16X objective (0.8NA, Zeiss) using a Ti:Sapphire laser (DeepSee, Spectra-Physics) tuned to 920 nm. PrairieView software controlled a resonant scanner of a multiphoton microscope (Ultima Investigator microscope, Bruker). Fluorescence was collected through a green emission filter (et525/70m-2p, Chroma Tech, VT, USA) and detected by a GaAsP PMT (Hamamatsu Model H10770). Image sequences over a 512 x 512 µm field of view were captured at 7.5 Hz in layer 2/3.

Each imaging session targeted S1 or S2, which were located through the cranial window based on blood vessel landmarks and whisker mapping results (see **Intrinsic signal optical imaging**). The border area was avoided. In animals imaged more than once, no areas overlapped and only cells imaged in one session were included in the analyses. Five mice in total were imaged in both S1 and S2. However, in 3 mice, analyses were restricted to one region each due to poor GCAMP6S signal, occlusion of the window or not enough behavioral trials.

Image processing

Raw fluorescence images were pre-processed using Suite2p (https://suite2p.readthedocs.io/): regions of interest (ROIs) were selected and their fluorescence signals were extracted and deconvoluted. ROIs fluorescence traces for each experiment were visually confirmed and analyzed using custom MATLAB code. Fluorescence time-series were normalized to percent change from a time-varying baseline, which was thresholded and smoothed with a 4th-order, 81-point Savitzky-Golay filter (Dechery and MacLean, 2018).

Responsive cells and area under the curve analysis

Each imaging trial included a baseline period of 4 seconds before moving the texture into the whisker field. Responsive cells were defined as ROIs with a significant difference (Wilcoxon signed rank test, $p<0.05$) between the mean dF/F during the baseline period compared to the mean dF/F during the texture period, for any G5 and G0 texture trials, including sensory laser trials. Only responsive cells were used in subsequent analysis. Due to the slow kinetics of GCAMP6S and long sensory period of the task, we used area under the curve (AUC) of the dF/F trace as a measure of responsivity to the texture presentation. Texture responsiveness value was calculated as the AUC during the sensory period – AUC during the baseline period. Both periods were 3.8 seconds long. To determine the effect of the laser on cells that reduced response to the texture, any cell which showed negative texture responsiveness values during no-laser G5 trials had their other trial responsiveness values reversed in sign (**Fig. 2B**, bottom graphs).

Single-neuron discrimination index analysis

To quantify how well single cells could discriminate between the two hit and CR textures, a discrimination index (DI) was calculated based on neurometric functions using a receiver-operating characteristic (ROC) analysis (Chen et al., 2013, Chéreau et al., 2020). AUC of calcium signals during the second half of the stimulus presentation period minus the AUC of an equivalent baseline period in the G5 texture trials were compared to that of the G0 texture trials. ROC curves were generated by plotting, for all threshold levels, the fraction of G5 trials against the fraction of G0 trials for which the response exceeded threshold. Threshold levels were defined as a linear function from the minimal to the maximal calcium signals. DI was computed from the area under the ROC curve by: $DI = (AUC-0.5) \times 2$. DI values vary between −1 and 1. Positive values indicate a larger response, or selectivity, to the G5 texture compared to the G0 texture, whilst negative values indicate a selectivity to the G0 over G5 texture. DI values above chance were assessed using permutation tests, from which a sampling distribution was obtained by shuffling the texture labels of the trials 1,000 times. The measured DI was considered significant when it was outside of the 2.5th–97.5th percentiles interval of the sampling distribution.

Anatomical Verification of the S1 L5 to POm to S2 Pathway

With reference to **Suppl. Fig. 1**, we used anatomical tracing to identify the area of POm that received S1 layer 5 terminals and contains POm cells which project to S2. Rbp4-Cre mice were injected with Cre-dependent Jaws-TdTomato and implanted with a head bar and cranial window above S1 and S2, as described in **Surgical procedures**. IS imaging was performed to identify S1 and S2 (see **Intrinsic signal optical imaging**) and 80nl of the retrograde tracer, FluoroGold, was injected into S2. One week later, the mice were perfused and sectioned to locate the region of POm with overlapping Jaws-TdTomato and Fluorogold cell body expression.

Fluorescence Microscopy

All mice used in behavioral, electrophysiological and anatomical experiments were perfused with cold, phosphate buffered saline (pH 7.2, 50ml) followed by cold, 4% paraformaldehyde (100ml). Brains were extracted, sucrose-protected over two days, and sectioned on a sliding microtome. Brain sections were cut 50µm thick and mounted with Superfrost slides. Some fluorescent photos were captured before mouting. Fluorescence signals were visualized under a fluorescence microscope (Leica Microsystems) using the appropriate filter cubes. Images were captured using a Retiga-2000 CCD monochrome camera and QCapturePro imaging software (Teledyne QImaging, Surrey, BC). Image post-processing such as estimating the distance from optic fiber implant (**Fig. 2J**) was performed with ImageJ software.

IN VIVO ELECTROPHYSIOLOGY

With reference to **Suppl. Fig. 2**, we validated Jaws opsin inhibition at S1 L5 to POm terminals. Jaws and ChR2 was expressed in S1 L5 neurons by injecting 450nl of a 1:1 mix of AAV8-CAG-FLEX-Jaws-KGC-TdTomato-ER2 and AAV5-DIO-ChR2-eYFP (UNC Vector Core) in Rbp4-Cre mice (n=4). After 3 - 4 weeks, mice were anesthetized with urethane (1.3mg/g) and a 6mm x 5mm craniotomy was made over S1 and POm. A 473nm LED was placed over S1 (ML: 3.1mm, AP: -0.8) and multiunit recordings were made in POm (DV: −3.1, ML: +1.3, AP: −1.4 mm) using custom pulled tungsten-in-glass microelectrodes (1Mohm). The microelectrode was attached to an optic fiber implant (200µm diameter, 0.5NA, Thorlabs) such that the tip of the electrode was within 290µm of the end of the implant. The implant was connected to a 620nm LED (max 137mW/mm^2, PlexBright, Plexon). Custom Matlab code coordinated 473nm LED pulses (1Hz, 20msec long) and 620nm LED pulses (1-3sec long) with various relative onset times (50msec, 500msec, 1sec, 2sec). Signals were passed through a 300Hz high-pass and 12000Hz low-pass second-order Butterworth filter. The window for spike analysis was 6-40msec from the start of the 473nm pulse and spikes were thresholded to 5 standard deviations above baseline.

STATISTICS

Statistical tests were conducted in MATLAB (2020b) or Prism software (v.9, GraphPad). A Shapiro-Wilk test (<30 samples) or Kolmogorov Smirnoff test (>30 samples) was used to test for normality. If no significant departure from normality was found, parametric tests were used. For departures from normality, the non-parametric Wilcoxon signed rank test was used for unpaired values and the Wilcoxon matched-pairs signed rank test for paired values. Where normality differed for tests within an experiment, the more conservative non-parametric test was applied across the experiment for consistency. A significance level was set at 0.05 and multiple comparisons were adjusted with the Bonferroni correction unless otherwise indicated. Specific statistical tests used and sample sizes are indicated in figure legends and text.

ACKNOWLEDGEMENTS

We thank Adam Kunz, Jessica Manieson and Graham Fetterman for their technical assistance. This work was supported by the National Institutes of Health (Grants NS094184 and EY022388 to S.M.S. and F31EY031965 to C.McK.) and the National Health and Medical Research Council of Australia (Grant 2003646 to C.M.).

REFERENCES

Banerjee A, Parente G, Teutsch J, Lewis C, Voigt FF, Helmchen F (2020) Value-guided remapping of sensory cortex by lateral orbitofrontal cortex. Nature 585:245-250.

Berditchevskaia A, Cazé RD, Schultz SR (2016) Performance in a GO/NOGO perceptual task reflects a balance between impulsive and instrumental components of behaviour. Sci Rep 6:27389.

Blot A, Roth MM, Gasler IT, Javadzadeh M, Imhof F, Hofer SB (2021) Visual intracortical and transthalamic pathways carry distinct information to cortical areas. Neuron 109:1996-2008.

Bolkan SS, Stujenske JM, Parnaudeau S, Spellman TJ, Rauffenbart C, Abbas AI, Harris AZ, Gordon JA, Kellendonk C (2017) Thalamic projections sustain prefrontal activity during working memory maintenance. Nat Neurosci 20:987-996.

Chen JL, Carta S, Soldado-Magraner J, Schneider BL, Helmchen F (2013) Behaviour-dependent recruitment of long-range projection neurons in somatosensory cortex. Nature 499:336-340.

Chen JL, Voigt FF, Javadzadeh M, Krueppel R, Helmchen F (2016) Long-range population dynamics of anatomically defined neocortical networks. Elife 5.

Chen JL, Margolis DJ, Stankov A, Sumanovski LT, Schneider BL, Helmchen F (2015) Pathway-specific reorganization of projection neurons in somatosensory cortex during learning. Nat Neurosci 18:1101-1108.

Chéreau R, Bawa T, Fodoulian L, Carleton A, Pagès S, Holtmaat A (2020) Dynamic perceptual feature selectivity in primary somatosensory cortex upon reversal learning. Nat Commun 11:3245.

Danskin B, Denman D, Valley M, Ollerenshaw D, Williams D, Groblewski P, Reid C, Olsen S, Blanche T, Waters J (2015) Optogenetics in mice performing a isual discrimination task: measurement and suppression of retinal activation and the resulting behavioral artifact. PLoS One 10:e0144760.

Dechery JB, MacLean JN (2018) Functional triplet motifs underlie accurate predictions of single-trial responses in populations of tuned and untuned V1 neurons. PLoS Comput Biol 14:e1006153.

Felleman DJ, Van Essen DC (1991) Distributed hierarchical processing in the primate cerebral cortex. Cereb Cortex 1:1-47.

Gallero-Salas Y, Han S, Sych Y, Voigt FF, Laurenczy B, Gilad A, Helmchen F (2021) Sensory and behavioral components of neocortical signal flow in discrimination tasks with short-term memory. Neuron 109:135-148.e136.

Gerfen CR, Paletzki R, Heintz N (2013) GENSAT BAC cre-recombinase driver lines to study the functional organization of cerebral cortical and basal ganglia circuits. Neuron 80(6):1368-1383.

Gilad A, Helmchen F (2020) Spatiotemporal refinement of signal flow through association cortex during learning. Nat Commun 11:1744.

Gilad A, Gallero-Salas Y, Groos D, Helmchen F (2018) Behavioral strategy determines frontal or posterior location of short-term memory in neocortex. Neuron 99:814-828.e817.

Groh A, Bokor H, Mease RA, Plattner VM, Hangya B, Stroh A, Deschenes M, Acsády L (2014) Convergence of cortical and sensory driver inputs on single thalamocortical cells. Cereb Cortex 24:3167-3179.

Guo ZV, Inagaki HK, Daie K, Druckmann S, Gerfen CR, Svoboda K (2017) Maintenance of persistent activity in a frontal thalamocortical loop. Nature 545:181-186.

Helmchen F, Gilad A, Chen JL (2018) Neocortical dynamics during whisker-based sensory discrimination in head-restrained mice. Neuroscience 368:57-69.

Hilgetag CC, Goulas A (2020) 'Hierarchy' in the organization of brain networks. Philosophical transactions of the Royal Society of London Series B, Biological sciences 375:20190319.

Hong YK, Lacefield CO, Rodgers CC, Bruno RM (2018) Sensation, movement and learning in the absence of barrel cortex. Nature 561:542-546.

Javadzadeh M, Hofer SB (2022) Dynamic causal communication channels between neocortical areas. Neuron 110:2470-2483.e2477.

Kandel ER, Schwartz JH, Jessell TM (2000) Principles of Neural Science. New York: McGraw Hill.
Lacefield CO, Pnevmatikakis EA, Paninski L, Bruno RM (2019) Reinforcement learning recruits somata and apical dendrites across layers of primary sensory cortex. Cell Rep 26:2000-2008.e2002.
Lavallée P, Urbain N, Dufresne C, Bokor H, Acsády L, Deschênes M (2005) Feedforward inhibitory control of sensory information in higher-order thalamic nuclei. Journal of Neuroscience 25:7489-7498.
Le Merre P, Esmaeili V, Charrière E, Galan K, Salin PA, Petersen CCH, Crochet S (2018) Reward-based learning drives rapid sensory signals in medial prefrontal cortex and dorsal hippocampus necessary for goal-directed behavior. Neuron 97:83-91.e85.
Luo L (2020) Principles of Neurobiology, Second Edition: CRC Press.
Miller-Hansen AJ, Sherman SM (2022) Conserved patterns of functional organization between cortex and thalamus in mice. Proc Natl Acad Sci U S A 119:e2201481119.
Mo C, Sherman SM (2019) A sensorimotor pathway via higher-order thalamus. Journal of Neuroscience 39:692-704.
Musall S, Sun XR, Mohan H, An X, Gluf S, Li SJ, Drewes R, Cravo E, Lenzi I, Yin C, Kampa BM, Churchland AK (2023) Pyramidal cell types drive functionally distinct cortical activity patterns during decision-making. Nat Neurosci.
Nurminen L, Merlin S, Bijanzadeh M, Federer F, Angelucci A (2018) Top-down feedback controls spatial summation and response amplitude in primate visual cortex. Nat Commun 9:2281.
Odoemene O, Pisupati S, Nguyen H, Churchland AK (2018) Visual evidence accumulation guides decision-making in unrestrained mice. J Neurosci 38:10143-10155.
Park JM, Hong YK, Rodgers CC, Dahan JB, Harano N, Schmidt ER, Bruno RM (2022) Deep and superficial layers of the primary somatosensory cortex are critical for whisker-based texture discrimination in mice. bioRxiv:2020.2008.2012.245381.
Poort J, Wilmes KA, Blot A, Chadwick A, Sahani M, Clopath C, Mrsic-Flogel TD, Hofer SB, Khan AG (2022) Learning and attention increase visual response selectivity through distinct mechanisms. Neuron 110:686-697.e686.
Qi J, Ye C, Naskar S, Inácio AR, Lee S (2022) Posteromedial thalamic nucleus activity significantly contributes to perceptual discrimination. PLoS Biol 20:e3001896.
Reinhold K, Lien AD, Scanziani M (2015) Distinct recurrent versus afferent dynamics in cortical visual processing. Nature neuroscience 18:1789-1797.
Roland PE, Hilgetag CC, Deco G (2014) Cortico-cortical communication dynamics. Frontiers in systems neuroscience 8:19.
Schoenfeld G, Kollmorgen S, Lewis C, Bethge P, Reuss AM, Aguzzi A, Mante V, Helmchen F (2022) Dendritic integration of sensory and reward information facilitates learning. bioRxiv:2021.2012.2028.474360.
Sherman SM (2016) Thalamus plays a central role in ongoing cortical functioning. Nat Neurosci 19:533-541.
Sherman SM, Guillery RW (1998) On the actions that one nerve cell can have on another: Distinguishing "drivers" from "modulators". Proc Natl Acad Sci USA 95:7121-7126.
Sherman SM, Guillery RW (2013) Functional Connections of Cortical Areas: A New View from the Thalamus. Cambridge, MA: MIT Press.
Squire LR, Berg D, Bloom FE, du Lac S, Ghosh A, Spitzer NC (2008) Fundamental Neuroscience, Third Edition: Academic Press.
Takahashi N, Oertner TG, Hegemann P, Larkum ME (2016) Active cortical dendrites modulate perception. Science 354:1587-1590.
Takahashi N, Ebner C, Sigl-Glöckner J, Moberg S, Nierwetberg S, Larkum ME (2020) Active dendritic currents gate descending cortical outputs in perception. Nature neuroscience:10-0677.
Theyel BB, Llano DA, Sherman SM (2010) The corticothalamocortical circuit drives higher-order cortex in the mouse. Nature neuroscience 13:84-88.

Trageser JC, Keller A (2004) Reducing the uncertainty: gating of peripheral inputs by zona incerta. J Neurosci 24:8911-8915.
Usrey WM, Sherman SM (2021) Exploring Thalamocortical Interactions: Circuitry for Sensation, Action, and Cognition. New York: Oxford University Press.
Vezoli J, Magrou L, Goebel R, Wang XJ, Knoblauch K, Vinck M, Kennedy H (2021) Cortical hierarchy, dual counterstream architecture and the importance of top-down generative networks. Neuroimage 225:117479.
Wichmann FA, Hill NJ (2001) The psychometric function: I. Fitting, sampling, and goodness of fit. Percept Psychophys 63:1293-1313.
Yang H, Kwon SE, Severson KS, O'Connor DH (2016) Origins of choice-related activity in mouse somatosensory cortex. Nat Neurosci 19:127-134.